Lipid-membrane protein interaction visualized by cryo-EM: a review

Valérie Biou

Lipid-membrane protein interaction visualized by cryo-EM: a review

Valérie Biou

Laboratoire de Biologie Physico-Chimique des Protéines Membranaires, UMR 7099, CNRS/Université de Paris, Institut de Biologie Physico-Chimique (IBPC, FRC 550), 75005 Paris, France

For correspondence: Valérie Biou, valerie.biou@ibpc.fr

Abstract

Membrane proteins reside at interfaces between aqueous and lipid media and solving their molecular structure relies most of the time on removing them from the membrane using detergent. Luckily, this solubilization process does not strip them from all the associated lipids and single-particle cryo-transmission electron microscopy (SP-TEM) has proved a very good tool to visualize both protein high-resolution structure and, often, many of its associated lipids. In this review, we observe membrane protein structures from the Protein DataBank and their associated maps in the Electron Microscopy DataBase and determine how the SP-TEM maps allow lipid visualization, the type of binding sites, the influence of symmetry, resolution and other factors. We illustrate lipid visualization around and inside the protein core, show that some lipid bilayers in the core can be shifted with respect to the membrane and how some proteins can actively bend the lipid bilayer that binds to them. We conclude that resolution improvement in SP-TEM will likely enable many more discoveries regarding the role of lipids bound to proteins.

Keywords: cryo-electron microscopy, membrane protein, phospholipid, density map, model building.

Introduction

Natural membranes have diverse compositions according to their host organism, (sub-)cellular localisation and time, but are most of the time rich in phospholipids with glycerol-related head groups and aliphatic chains, with a small number of insaturations. Due to their special shape, cholesterol in eukaryotes, and cardiolipin in bacteria and mitochondria contribute to membrane shape changes and diversity. Structures of membrane proteins up to now, have mostly been solved using protein solubilised in detergent and stabilised with either detergent micelle, amphipol or nanodisc. Those devices act as buoys and allow the protein to be in a stable conformation and to keep a limited number of associated lipids. Analogous to water molecules in soluble protein regions, lipids associated with membrane proteins can be divided into four groups: bulk lipids that do not interact or have transient interactions with the protein, so-called annular lipids that form a first shell around the protein, usually consisting of a single layer, lipids located in grooves on the protein surface, often at the interface between subunits, and buried lipids that are bound inside the protein core.
Bulk lipids are fluid and do not appear in X-ray or single-particle cryo-electron microscopy (SP-TEM) structures, either because they have been removed during the solubilization process in detergent, or because they are in fast equilibrium and do not have an ordered location. Annular and groove lipids,

on the other hand, are sometimes present even after detergent solubilization and can be co-purified from the expression medium or added during nanodisc reconstitution.

In the last ten years, the Protein Data Bank (PDB) has seen an ever-increasing amount of membrane protein structures solved to high resolution by SP-TEM thanks to the recent improvements in instrumentation and methods.

Whereas atomic resolution structural methods can describe lipid location, the following biophysical methods are complementary for analytical and quantitative characterisation.

i) EPR studies of protein-bound lipids showed early-on the presence of annular lipids and allowed to determine the preference of proteins for some lipids [1–3]. Ii) Solid-state NMR is a good tool to study protein-lipid contacts weaker than those observable via crystallography or SP-TEM, and describe the dynamics of their interactions; see [4] for a review. Iii) Native mass-spectrometry is another tool to provide lipid-protein interaction information that are complementary to high-resolution structures (reviewed in [5]). Iv) Lipids co-purified with the protein can also be extracted with chloroform and identified by mass spectrometry measurements (for example [6]).

Reviews published in the early 2000's described well-ordered lipids bound to high resolution X-ray structures [3,7]. They undergo two types of lipid-protein interactions: polar contacts involving their head groups mostly bound to basic aminoacids, and van der Waals contacts via their hydrophobic tails. As X-ray diffraction comes from the interaction of a very large number of protein molecules (of the order of 10^{10} molecules) regularly arranged in a crystal, the density of lipids at positions with low frequency of occupation at a given location may be erased. In practice, only a few, well-ordered, lipids are visible in X-ray density maps.

SP-TEM has several advantages to visualise lipids: i) it allows protein direct extraction from its native membrane using styrene-maleic acid copolymer (SMA) nanodisc [8] or other polymer such as amphipol [9], whose charge would not allow crystallization but is not detrimental to SP-TEM. However, to this time, only 25 SP-TEM structures produced from SMA native extraction are deposited in EMDB, with reduced protein variety and we did not include any in this review. Ii) solubilization with low-critical micellar concentration detergents (lauryl-maltose neopentyl glycol, LMNG for example) keeps a proportion of native lipids or allows addition of phospholipids known to stabilize the protein or complex. iii) it relies on averages of fewer protein particles, of the order of hudreds of thousands rather than billions for a crystal. This probably enables to better keep the relative location of lipids with respect to protein and therefore to observe the bound lipids in SP-TEM maps.

Recent SP-TEM maps revealed a wealth of non-protein densities in the membrane area that is often likely associated to lipids but is sometimes overlooked in structure papers. In this review, we would like to explore the visualization of lipids on SP-TEM maps, and describe which are the best conditions to observe them in terms of resolution and symmetry. We will also compare lipid visualization using X-ray electron density maps and cryo-EM maps for some proteins. We will first analyse lipid visualization in different circumstances *via* an example: the ExbB pentamer from *Serratia marcescens*. We will consider the influence of the symmetrized map in different regions of the protein, and determine at what density levels lipids and protein can be observed, and compare maps at different resolutions. Next, we will visualise ordered lipids in different membrane proteins and complexes from density maps

available publicly in the Electron Microscopy Data Bank (EMDB) [10] and try and determine the conditions for lipid visualization and their functional importance. It must be emphasised that it is difficult to identify lipids from detergent molecules and what is called “lipid” in the text is a molecule whose shape is compatible with a phospholipid molecule, but may as well be a detergent.
In view of the many recent membrane protein structures published and deposited in the PDB [11] and EMDB, this is by no means an exhaustive review; instead, we tried to observe structures with high resolution densities and we apologise for the many omissions.

Methods

Membrane protein structures solved by SP-TEM at resolutions better than 3.5Å were selected in the protein data bank and the associated map was downloaded from EMDB using the link provided in the PDB. Some additional structures with lower resolution were used in complement to the higher resolution ones when judged appropriate (for example, when most closed states had high resolution, an open state with lower resolution was downloaded). The model protein chains were colored using “Rainbow chain” command; most of the time, the non-protein residues were colored black. The figures showing “Tube helix” representation of the PDB model are made with UCSF ChimeraX [12].The PDB model and the map were loaded into UCSF Chimera [13]. The SP-TEM map was colored according to the model using the “Scolor zone” command. This results in leaving the non-modelled map in the original color (most of the time light grey or cream) and this allows to outline the non-modelled associated lipids on the colored background of the model-associated map. Images of the model and of the associated map were taken, then slices at different density levels and thickness were selected to outline the lipids in different sites. The level at which the map is traced is indicated in the figure legends, according to [14] (see example in Figure 1A). Table 1 gives a list of all PDB and EMDB identifiers used in the figures, along with resolution, symmetry and associated literature reference. Supplementary Table 1 lists the same PDB identifiers with the non-protein ligands, in particular detergent, lipids and aliphatic chains that were traced in the trans-membrane regions. They display a large variety showing the authors’ choices to interpret density maps.

Visualizing lipids in an SP-TEM density map: level and influence of symmetry.

We found it difficult to rationalise at which contour level of density the lipids could be seen. In practice, very few deposited maps are normalised and no threshold can be considered universal. We used the contour level references introduced in the review published by Zampieri et al. [14]. They use the density distribution profile that has a characteristic bell-like shape and identify four contour levels with 0 corresponding to the strongest density (where the ordered protein regions are visible), 1 to the level at which the ordered lipids are visible and the detergent/nanodisk density belt appears, and 2 is the level at which the detergent/nanodisk buoy is very visible. A fourth level is defined, where the map is very noisy (figure 1A). We decided to use this level definition and indicated it in the figure legends.
The *Serratia marcescens* ExbB (PDB ID: 6YE4 [6]) SP-TEM map observed at a density level corresponding to level 1, or 10 root mean square deviations (RMS), shows a clear protein density and one phospholipid density per monomer (coloured black, figure 1-B). Additional density is visible but not

clearly connected (figure 1-B). The same map observed at 5 RMS (level 2) shows the detergent micelle (figure 1-C) and a bilayer-like density inside the pore.

When symmetry is imposed on EM density maps, it may erase lipid positions with low occupancy or fuzzy location similarly to X-ray density maps. ExbB is a homopentamer with one ordered phospholipid (identified as mostly phosphatidyl glycerol (PG) via mass spectrometry [6]) per monomer. The C1 map with no symmetry applied and the C5 map (to which a 5-fold symmetry was applied) are very similar with 98% correlation according to UCSF Chimera [13]. Still, the maps show some differences, particularly in the lipid region. The C5 Map global aspect shows the annular lipid bilayer (Figure 1-C). Figure 1-D shows the non-symmetrised map for comparison: the lipids are less clearly visible. Looking around one of the ordered PG molecules, one can see a strong difference between C5 (figure 1-E) and C1 (figure 1-F) maps. Both maps show additional density that can be assigned to lipid chains (coloured white on figure 1-E and grey on figure 1-F). The C5 map shows more details than the C1 map but both are interpretable. The C5 map does not seem to be biased by the symmetry in this area. It is clear that the density is reinforced when the symmetry is respected, but it can be blurred if there is a slight shift of the molecules.

The density inside the pore is almost invisible at the level 1 but appears at level 2. It has the shape of a bilayer that is shifted towards the periplasmic region with respect to the micelle. The bilayer is less clearly drawn in the C5 map (figure 1-G) than in the C1 one (figure 1-H), especially in the periplasmic leaflet, probably because this region does not obey the protein symmetry and that symmetry imposition erases part of the signal. This is less obvious in the annular density because the ordered lipids are located close to the protein which respects the symmetry constraints (compare figures 1 D and E). It is therefore advisable to compare the maps with and without symmetry.

Finally, we compared X-ray and SP-TEM information about lipids: $ExbBD_{ec}$ X-ray maps 5SV0 and 5SV1 (4Å resolution) do not show any information about lipids (both internal and external), similarly to the SP-TEM map of 7AJQ (4Å resolution), whereas higher resolution maps for 6TYI (3.3Å resolution) and 6YE4 (3.2Å) show ordered lipids. Using this example and others, it seems that lipids are visible only at resolutions better than 3.5Å.

In conclusion, symmetrised maps may help bring details to light when the model respects the symmetry relationships, but it can also blur details that don’t respect it. Moreover, symmetry always breaks at a point in resolution and may therefore erase information about minority conformational states.

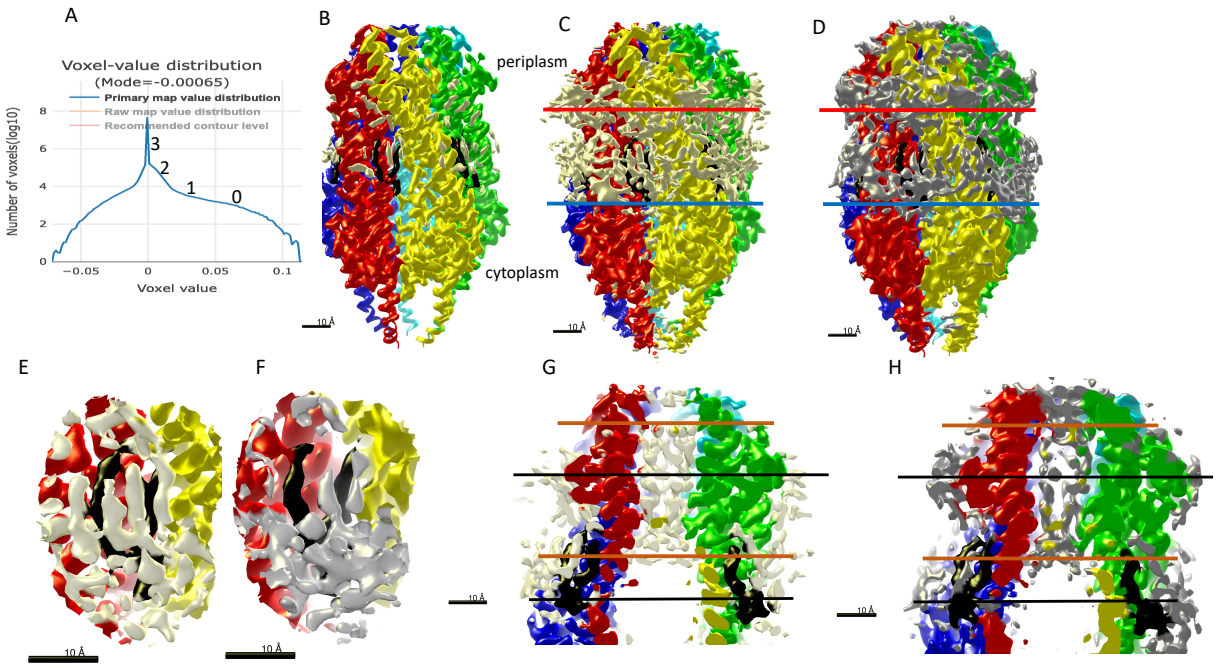

Figure 1
ExbB pentameric symmetry influences map aspect. The protein monomers are colored blue, cyan, green, yellow and red, the lipid is colored black and the associated maps are colored accordingly. A, Validation histogram for EMDB-10789 with location of contour levels as defined in [14]. B, ExbBB (PDB ID: 6YE4) map with C5 symmetry displayed at level 1 according to shows the protein density and one lipid per monomer. C, ExbBB map with C5 symmetry displayed at level 2 to show part of the annular lipids. D, ExbBB map with C1 symmetry displayed at level 2 shows a similar view. E - F, focus on the lipid density at the interface of two monomers (level 2). E, C5 map and F, C1 map. The protein monomers are coloured red and yellow; the PG molecule is in dark grey; the maps are coloured according to the model and the non-modelled density regions are transparent grey and orange respectively. G-H: view across the channel at level 2 shows the inner bilayer between black lines and the micelle between orange lines.

Ordered lipid-binding sites description and function

In the following sections, we observe PDB models and SP-TEM maps from the EMDB for chosen families and will comment on the bound lipids: their location, visibility and what is known about their contribution to the protein function.

Ordered lipids in bays or clefts at interfaces between monomers

Probably because they are more sheltered from the bulk micelle, more ordered lipids are visible in more buried locations such as close to monomer interfaces, or even buried in the interface, thus mediating protein-protein interaction.

Transient receptor potential channels

- Transient receptor potential vanilloid (TRPV) channels respond to a variety of stimuli ranging from heat to cannabis and trigger many subsequent signaling pathways upon activation. This family is a very good study subject for our review, as many structures have been deposited by different groups and lipids are visible in annular, cleft or buried sites. Very few crystal structures of the full protein have been solved and, to our knowledge, no model had lipids in it; on the other hand, anomalous diffraction identified a metal ion strongly bound to the protein [15]. Such identification is not possible using electron microscopy. Since the development of SP-TEM and HEK293 cell expression system, this

family of proteins has been studied in depth thanks to many structures with resolutions better than 3Å, see [16] for a review.

TRPV6 protein is a tetramer with six transmembrane helices per monomer that form a pore, and a cytoplasmic domain with ankyrin repeats. Structure PDB ID: 7S88 is in glyco-diosgenin detergent [17], figure 2-A-B). It is coated with many lipids, showing that mild detergent allows strongly-bound lipids to remain tied to the protein. Their location is at the interface between monomers that form a rather shallow bay (figure 2-C). As shown with the electrostatic surface coloring, the phospholipid head chains are in contact with polar residues and their aliphatic chains are in contact with hydrophobic regions (figure 2-D). Figure 2-E shows a detail of density map traced at level 1 of the phospholipid bilayer at the interface of two monomers and figure 2-F shows the associated model. The region of this map is rather exceptional in that it shows lipids from both leaflets in close proximity. The lipid head is more disordered and is visible only at lower density level. The protein was purified in a buffer containing cholesterol hemi-succinate (CHS) and three densities per monomer have cholesterol-like shapes (as exemplified on figure 2-G with associated model on figure 2-H). The CHS molecules are buried in hydrophobic pockets inside the protein and interact with one or two monomers, in this case mediating the interface.

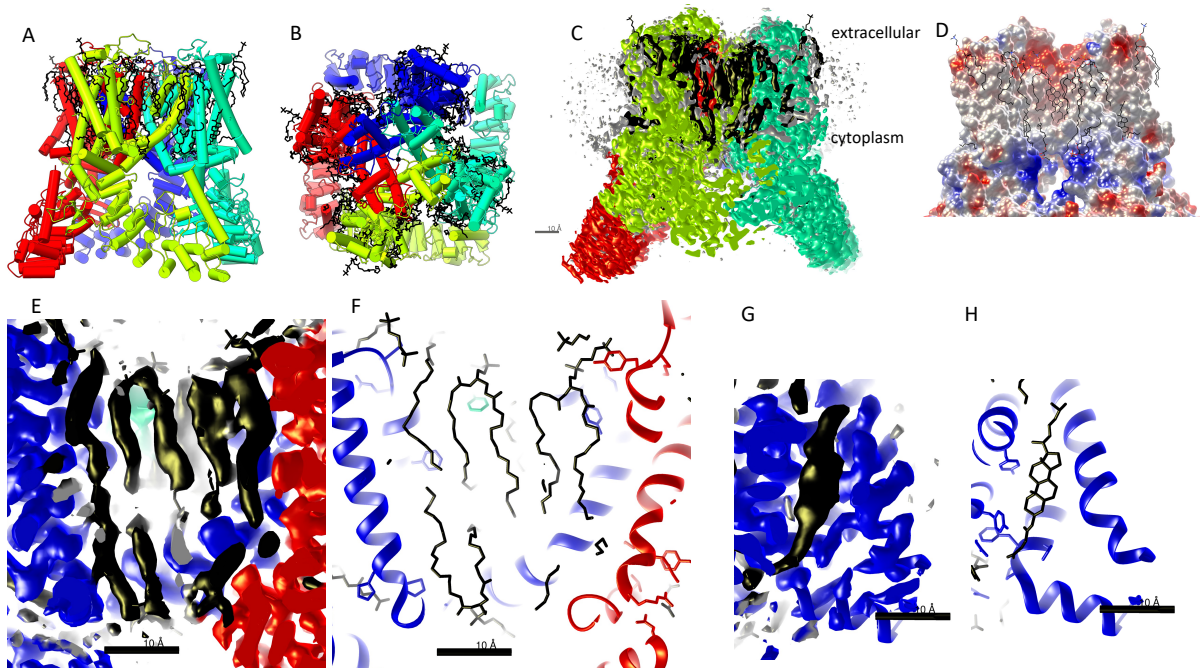

Figure 2
TRPV6 and associated lipids. A-B, the model is colored according to the protein chains in red, yellow, blue and green, the traced lipids are colored black and the map is colored according to the associated model and the unmodelled density is grey. C, cholesterol, lipids in a cleft between 2 monomers: map traced at level 1. D, model surface colored using the electrostatic potential: blue, positive; red, negative. E-F, model and map around another cholesterol; G-H, model and map around ordered lipids forming a bilayer.

Similarly, the TRPV5 protein (PDB ID: 6O1N [18]), was purified in the absence of any added cholesterol or cholesterol hemi-succinate (CHS), and also shows cholesterol-like density that is likely endogenous. This is also the case in structures of TRPV6 in nanodisc 7S89, or in amphipol 7S8C [17], although the number of visible ordered lipids is lower, irrespective of the overall resolution.

In summary, TRPV structures show part of a bilayer in the annular region and specific binding of lipids and cholesterol in the protein core can be visualised, both in detergent and in nanodisc.

- F0F1 ATP synthase

The F0F1 ATP synthase is a rotatory motor that reversibly couples a proton-motive force (pmf) generated by respiration to the synthesis of ATP from ADP and phosphate. X-ray crystallography revealed the extraordinary machine structure and its different states and earned the Nobel prize awarded to Paul Boyer, John Walker and Jens Skou for P-type ATPase. The reaction is energised via a rotatory mechanism that involves a rotor made of a nine c-subunit cylinder. This cylinder interacts with subunit a in the membrane, and subunit a itself interacts with two TM helices of subunits b in the F0 subcomplex [19]. The pmf provides energy for ATP production from ADP + Pi in the F1 complex (figures 3 A and B) [20]. For more precise structural description of the F-type ATPases, see [21].
SP-TEM high-resolution density maps provide images of lipids associated with the proteins, often at interfaces between subunits. Here we will focus on the F0 sub-complex that is located in the inner membrane of gram-negative bacteria, of chloroplasts or mitochondria. A density observed inside the subunit c undecamer cylinder is difficult to interpret: is it lipid or protein (black oval on figure 3 C)? Its size is compatible with a lipidic bilayer but its shape is not that of phospholipids.
In high-resolution structures such as 7NK9 (figure 3 D-G) and 7NL9 (figure 3 H-I) [22], the density between subunit a and two subunits c is reminiscent of a lipidic monolayer that rests on subunit a. The volume of this monolayer varies according to the rotatory state of the complex (compare figures 3 F in state 1 and I in state 3). The SP-TEM map clearly shows this phenomenon, even though the molecular modelling of individual lipids is not easy due to the lower resolution of this area.

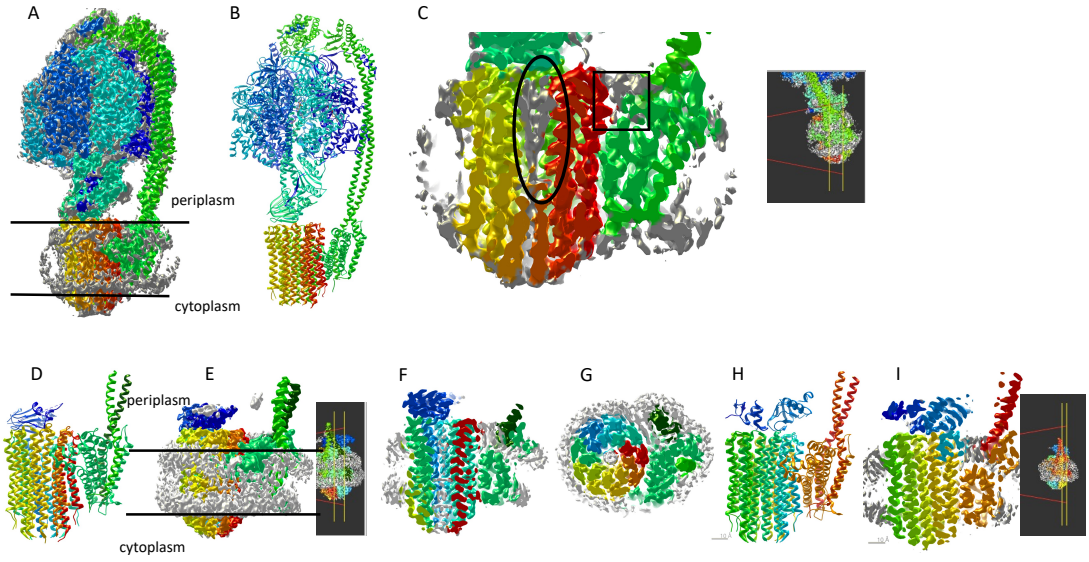

Figure 3
Structure and lipid interaction of bacterial F0F1 ATP synthase. A-C, structure 7JG5. A, density map traced at level 1 colored according to the corresponding subunits. The grey regions correspond to zones that are distant from protein atoms. This enables us to locate the micelle. B, protein model with the same color. C, slice of density at a lower level showing the density in the core of the c subunit undecamer (yellow and red), the density inside the undecamer (black oval) and the density at the interface between the red c subunit and the green a subunit (black box). D-G, PDB ID: 7NK9 showing state 1 of F0. D, model with chains colored differently. E, density map traced at level 2 colored according to the corresponding subunits; the black-background inset shows the volume slice selected. F, slices cut into the membrane area show the protein and lipid density compatible with a monolayer in grey (black box) between the subunits c (yellow-green-cyan), subunit a (orange) and subunit b (red). G, perpendicular view to F. H-I, PDB ID: 7NL9 showing state 3 of F0. H, model with chains colored differently. I, slices cut into the membrane area show the protein and lipid density compatible with a monolayer in grey (black box) between the subunits c (yellow-green-cyan), subunit a (orange) and subunit b (red).

While bacterial and chloroplastic ATP synthases are monomeric, dimer formation in mitochondrial ATP synthases induces membrane curvature. Murphy et al. have solved several states of mitochondrial ATP synthase [23]. Figure 4-A shows the density of a dimer with one complex colored. Figure 4-B shows the associated model. Figure 4-C shows a slice of density seen at low density level near the interface between c subunits (green), subunit 6 (magenta) and ASA6 subunit (cyan), and the second complex colored grey. Similarly to bacterial ATPase, the lipid builds a single monolayer (Figure 4-C,brown box). In addition, a bilayer of a few phospholipids is visible at the interface between both complexes, forming a hinge in the TM region that deforms the membrane (rectangle in Figure 4-C, black box).

In summary, SP-TEM maps reveal the presence of ordered lipids in contact with several interfaces of the ATP synthase subunits. Their function has not been described yet. They could help the rotation of subunit c assembly and certainly deserve further studies. As an example, molecular dynamics studies could provide information.

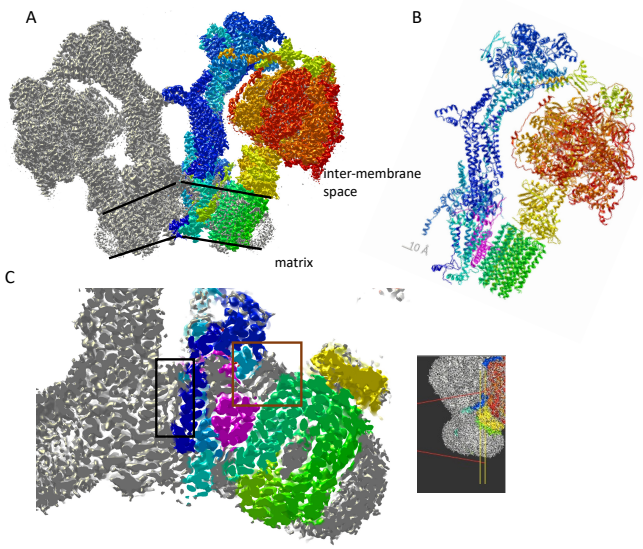

Figure 4
Dimeric mitochondrial ATP synthase PDB ID: 6RD4. A, level 1 representation of density map shows a dimer. The left complex is left in grey and the right complex is colored according to protein chains in the model (figure 4 B). The lines depict the TM regions in both complexes. B, model colored according to protein chains in one complex. C, viewed at level 3, density slice passing through the interface between c subunits (green), subunit 6 (magenta) and ASA6 subunit (cyan), brown box on the one hand and the interface between subunits forming the dimer (black box) on the other hand. the black-background inset shows the volume slice selected.

specific binding sites: lipids as substrate or effectors of membrane proteins

ion channels MscS

Bacteria protect themselves from sudden osmotic shock via mechano-sensitive channels of large and small conductance (MscL and MscS) that open when membrane tension increases. MscS are heptamers with a large cytoplasmic domain and three TM helices per monomer. Many X-ray structures have been published since 2007. They show both open and closed states of the channel with few associated acyl chains and complementary biophysics studies showed a role of lipids in the gating mechanism [24]. Most of the published SP-TEM structures are in a closed state. We decided to compare 6VYK and 6VYL structures as they have resolutions of 4.2 and 3.4Å and are in closed and

partially open states, respectively. Lipids are viewed in pores, pockets and vents [25]. Figures 5 A and B show MscS closed structure 6VYK with lipid models. The associated density map shows lipid density located in the membrane pore, at the level of the cytoplasmic leaflet of the micelle (figure 5-C). One annular lipid has very clear density at the interface between monomers. It is named Gatekeeper lipid by the authors and stabilises the closed conformation of the protein (figure 5-D). This density is located at the level of the cytoplasmic leaflet and no associated ordered density is visible on the periplasmic side. Structure 6VYL is one of rare partially open structures with ordered density in the membrane area (figure 5 E-F). It was obtained in the presence of phosphatidyl choline lipid with shorter tails of 10 Carbon atoms as compared to 18 for 6VYK [25]. This could indicate that thinner membranes could trigger MscS opening, however, the authors have not been able to show this. Due to sliding of the TM helices with respect to each other, the transmembrane region of the protein is less thick, has no gatekeeper lipid, and the pore also shows lipid density with a larger surface area and located closer to the periplasm (compare figures 5 C and G). In both structures, C7 symmetry was applied during map calculation and may change the channel lipid visualisation, as seen for ExbB. MscS is thus able to induce order in the lipids inside its channel.

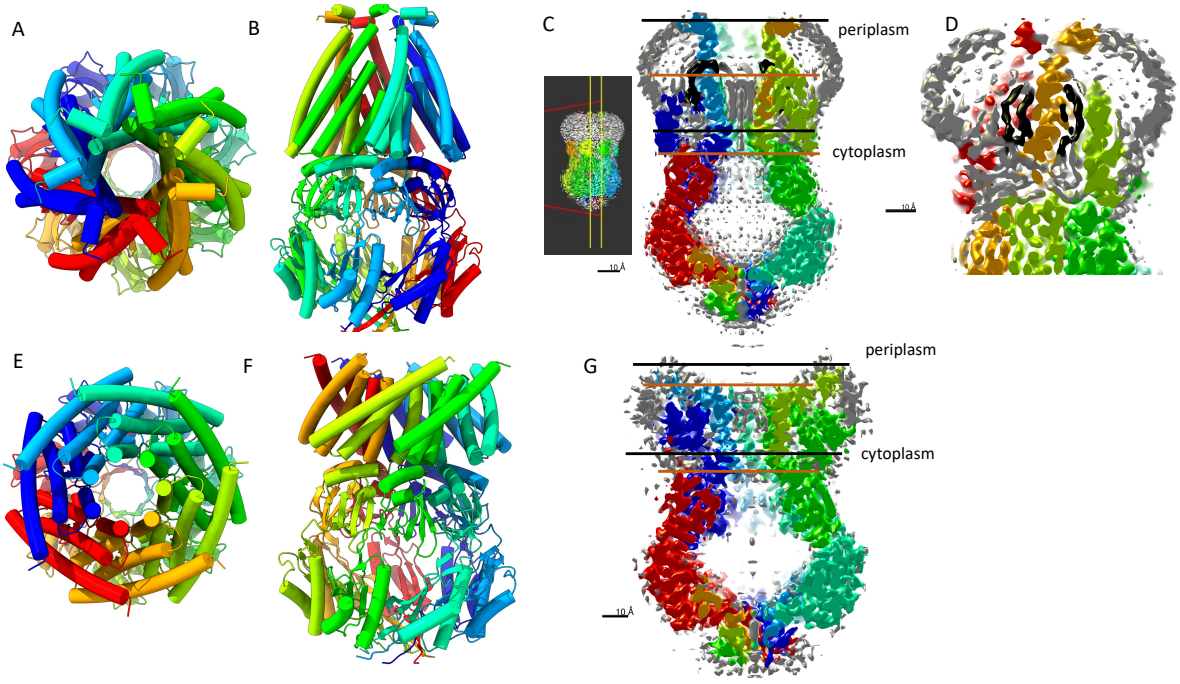

Figure 5
Mechanosensitive channel MscS. A-D, PDB ID: 6VYK in closed state. A and B, top and side views of the heptamer model colored according to their aminoacid chains. C, density map traced at level 2 across the channel. the black line shows the limits of the nanodisc and the orange line shows the limits of the inner bilayer. D, a second slice of density through the channel shows ordered lipids at the interface between monomers. E-G, PDB ID: 6VYL, partially open state of MscS. E and F, top and side views of the heptamer model colored according to their aminoacid chains. G, density map raced at level 2 across the channel. The black line shows the limits of the nanodisc and the orange line shows the limits of the inner bilayer. The insets illustrate the location of the displayed slice.

Lipopolysaccharide transport complex Lpt

Lipopolysaccharide (LPS) is a large glycolipid consisting of lipid A, core oligosaccharide and O-antigen and it is the main component of the gram-negative bacteria outer membrane. It is synthesised in the IM and transported via an ATP-binding cassette transporter Lpt complex to the OM. The Lpt crystal structures did not reveal LPS binding but showed that IM subcomplex is made of LptF and LptG

subunits with 6 TM domains and 2 alpha-beta cytoplasmic ATPase LptB subunits; the higher-resolution structures showed a few aliphatic chains bound to the membrane area [26]. Then high-resolution SP-TEM structures showed lipid and LPS positions in different stages of the transport reaction. We chose to illustrate this part with reference [27], which shows three steps of LPS transport. In a first step (PDB id: 6S8N [27] figure 6 A), the LPS binds rather weakly in the presence of subunit LptC whose TM helix transiently interacts with the complex. 6S8N structure shows an extended network of non-protein density in the cytoplasmic membrane leaflet that is assigned to detergent molecules but could also be lipids (figure 6 B-C). The “lipids/detergent” molecules are located on both sides of the cytoplasmic leaflet, not exactly opposite the LPS. In the next step (PDB id: 6M8H [27]), LptC binding is destabilized by LPS and leaves the complex, allowing for the cleft between both subunits LptF to close down and push the LPS up (figure 6 D-E) so that it may interact with other periplasmic partners for its ascension to the OM. The LPS binding site of 6M8H overlaps with that of 6S8N and it extends further to the periplasm and interacts more strongly with a cleft of LptB. The LPS aliphatic region rests on a “floor” formed by protein and non-protein densities. Part of the aliphatic chains of LPS interact with the protein, while others, on both sides of the protein, face other aliphatic chains traced as detergent in the model. In a third step, 2 ATP molecules are hydrolysed in the B subunits and the LPS is released for a next cycle to occur (PDB id: 6S8G, figure 6 F-G [27]). The membrane subunits are in closed conformation and only one lipid aliphatic chain is visible.
In conclusion, SP-TEM of Lpt revealed the different steps of LPS transfer to the periplasm, showing a movie of its capture, ascension and release. Free lipids are rare in these structures, and no annular lipids are observed but the LPS is visible with exquisite details.

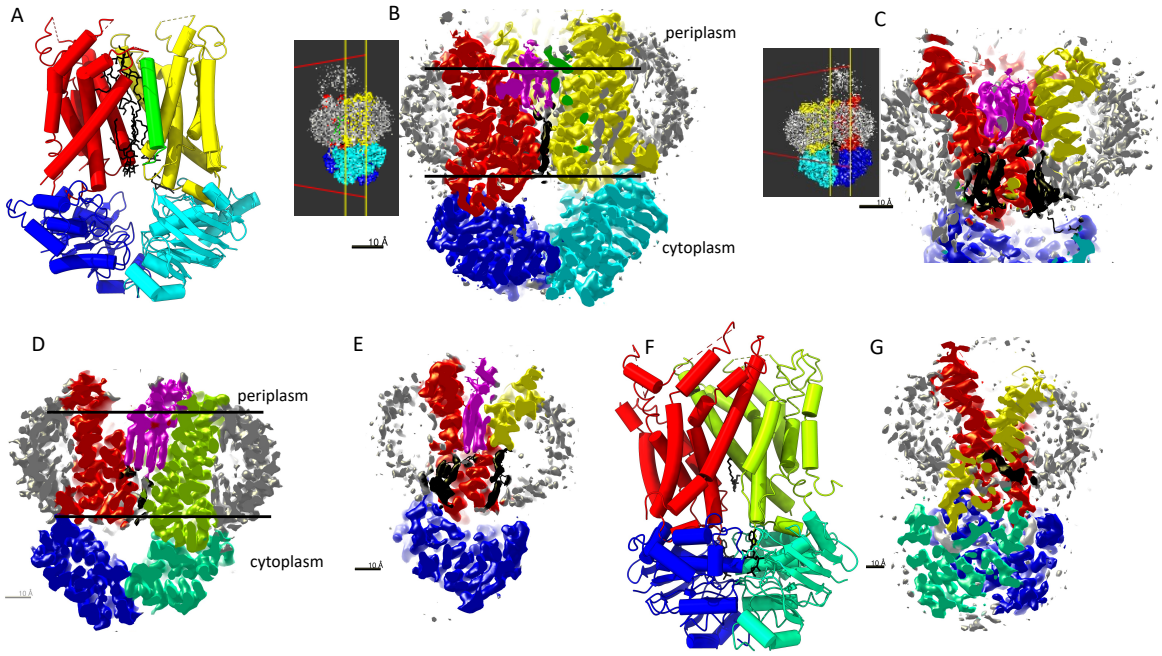

Figure 6
Lipopolysaccharide export system. LptB2FG ABC Transporter. Subunits B are in bue and cyan, subunit F in yellow, G in red and subunit C is green. The LPS is magenta and other lipids are black. A-C, 6S8N-EMD10125 complex with the C subunit. A, model of the protein; B-C, corresponding SP-TEM map traced at level 2 shown in different slices as indicated in the incept. D-E, 6S8H-EMD10122: complex after C subunit dissociation. the LPS moiety appears larger and closer to the periplasmic side than on figure 7-B. D, part of the aliphatic chains of the LPS face those of detergent; E, others face the protein. F, model 6S8G and G, map EMD10121 of complex after LPS dissociation and ATP hydrolysis (white density in cytoplasmic subunits).

- eukaryotic RND transporters with sterol-sensing domain

The resistance-nodulation-division (RND) family of membrane proteins exists in bacteria and eukaryotes. It couples pmf with biomolecule transport and is often involved in drug (antibiotic or chemotherapy) efflux. Lipids are visualised outside and inside the assemblies and play crucial roles in the function.

The known members of the RND family in eukaryotes have a pseudo-symmetry in the 12 TM helical domains and two large ectodomains. They share a sterol-sensing domain (SSD) in the first half of the TM region and are involved in cholesterol transport or binding.

The Hedgehog signalling pathway, crucial in embryo development and stem cell maintenance in animals, is controlled by the N-terminal domain of the Hedgehog morphogen HhN, that is modified by a palmitic acid at the N-terminus and a cholesterol at the C-terminus. The Hedgehog pathway employs two RND proteins: Dispatched (Disp) in the emitting cells and Patched (or Patched homolog 1, Ptch1 in vertebrates) in the receiving cells. Their ectodomains are large, folded, post-translationally modified by glycosylation and stabilised by disulphide bridges and involved in the interaction with protein partners. No crystal structures were known of those proteins and the advent of SP-TEM and HEK293 expression triggered a boom of structures that started in 2018.

Patched1 is the receptor of Hedgehog, responsible for the concentration-dependent activation of the Hedgehog signalling pathway in receiving cells. The activation is linked to cholesterol transport [28]. In the adult, Patched1 is expressed in low quantities. It is a tumour suppressor in basal cell carcinoma and it is overexpressed in many cancers. It was shown to have a drug efflux function linked to chemotherapy resistance [29]. Several structures of mammalian Patched1 were published recently. In contrast to bacterial RND pumps, the structures of Patched1 show it as mostly monomeric, while dimers are bridged by HhN. All structures showed cholesterol-like densities bound in the membrane area and to the extracellular domains. The highest resolution structure (3Å) to date is 7RHR, a Patched1 structure from *Xenopus calcaratus* [30] and we chose it to illustrate this review. The monomer model shows three cholesterol molecules (black on figure 7 A) and the map shows additional annular lipids in the membrane area (off-white colour on figure 7 B). The three cholesterol densities are located in the ectodomain, in the “neck” region and in the outer membrane leaflet. This latter cholesterol density is accompanied by lipid-like elongated chains (figure 7 C). This chain of cholesterol densities can trace a path for cholesterol or drug efflux. Maybe due to the more limited resolution or because of lower affinity, annular lipids appear less ordered than for Disp.

Disp is located at the surface of Hedgehog-emitting cells and secretes lipid-modified HhN that transmits the signal to receiving cells. Disp is a monomer with a topology similar to that of Patched1 with an SSD in the first six TM helices and two large extracellular domains (figure 7 D). High-resolution structures such as 7RPI (2.5Å) are rich in ordered annular lipids forming a bilayer in the TM area (figure 7 E and F). Their shape is characteristic of cholesterol, probably cholesterol hemisuccinate (CHS) that was added during purification. The 7RPI model contains 28 lipids of which 26 are CHS [31]. Thus, it seems that Disp is able to accumulate tightly-bound cholesterol around itself forming a partial bilayer.

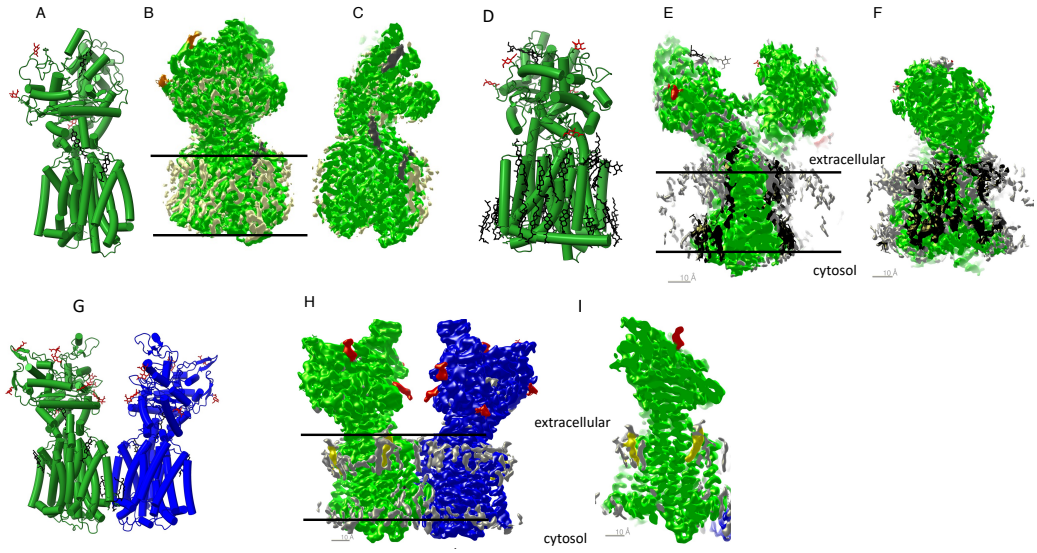

Figure 7
Eukaryotic RND proteins: Patched1, Dispatched1and NPCL1. A-C, Patched1 from xenopus 3Å structure 7RHR. A, protein model in green and non-protein residues in black and glycosylations in red. B, density map traced at level 1 shows protein density (green) and annular lipids (off-white). C, slice into the density shows 3 cholesterol binding sites (black). D-F, Dispatched1 PDB code 7RPI. D, protein model in green and non-protein residues in black. E, slice into the central density shows lipid bilayer around the TM area and cholesterol density. F, slice showing the external membrane region with annular lipids. G-I, NPCL1 structure 7N4U. G, dimer structure. H, density of the dimer colored green and blue with glycosylations in red, lipids in black and cholesterol yellow. The non-traced density is colored grey. I, slice into the density showing cholesterol binding in the external membrane leaflet.

NPC1 and NPC1L1: Niemann-Pick type C protein is involved in cholesterol homeostasis and its dysfunction is associated to lysosomal diseases. In the lysosome, low-density lipoprotein particles are cleaved from their cholesterol moieties. NPC2, a lysomal soluble protein, feeds NPC1 that transports cholesterol from the lysosome to the membranes of other organelles [32]. Several structures of NPC1 alone or with NPC2 have been solved by X-ray crystallography or SP-TEM. They show a 13-helical domain transmembrane region with a 13th helix as compared to 12-TM Ptch1 and Disp. The soluble lysosomal domains interact with NPC2 and a central tunnel enables cholesterol transport to the membrane [33]. Structure 6W5S of NPC1 in nanodisc [33] harbours no cholesterol in the membrane region, but elongated densities corresponding to a few annular lipids are visible (not illustrated here). Homologous NPC1-like1 protein is important for dietary cholesterol uptake in the intestine. Structure 7N4U [34] has the same fold as NPC1 in the membrane area and forms a dimer that interacts via the membrane regions (Figure 7G). Several annular lipids are visible at the surface and in the dimer interface (figure 7 H). It shows two cholesterols bound to the SSD regions of each monomer (figure 7 I).

In summary, the membrane region of eukaryotic RND transporters is surrounded with annular lipids or chlosterol with an ordered location. Similar to water molecules, they may have a role in the protein function, related to the acquisition of membrane-soluble substrates via the membrane such as cholesterol or hydrophobic drugs. They also harbour specific cholesterol binding sites in the SSD and other locations.

lipids inside protein channels

Some proteins form hydrophobic channels inside the membrane and lipid-like densities are sometimes visible inside those channels.

Rotors with 5:2 stoichiometry: ExbB-D

As discussed above, our ExbB structure from *Serratia marcescens* 6YE4 [6] shows density for at least one ordered lipid in clefts between 2 monomers (figure 8 A), similar to those seen in structure 6TYI. The order is better on the cytoplasmic leaflet, but the periplasmic leaflet also shows density. In the protein core and in the absence of ExbD, ordered density is visible when looked level 2 (figure 8 B). It closes the channel core and prevents ExbB from acting as a pore in the absence of ExbD. It is located higher than the micelle to the periplasm and is compatible with a lipid bilayer. Interestingly, this bilayer is located at the same level as the two TM helices of ExbD in the 7AJQ complex (Figure 8 C), [6]. We do not know if there is a functional reason for this shift of TM helices toward the periplasm, but we observe that it exists in MotAB [35] and E. coli ExbBD [36]. It could be related to the rotor function of those machines.

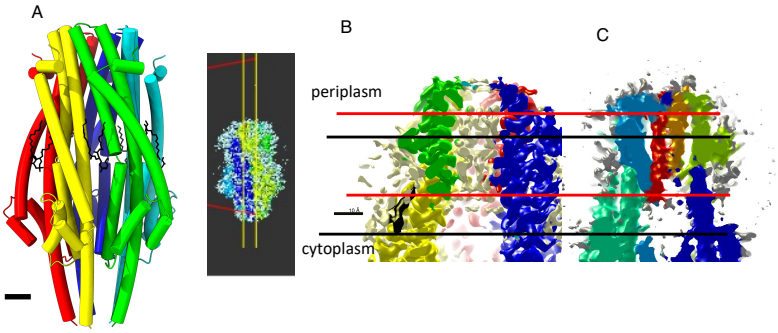

Figure 8
A-B, ExbB from *S. macescens* 6YE4. A, model colored according to protein chains. B, I, a slice of density map traced at level 2 inside the pentamer shows ordered lipid density. C, ExbB-ExbBD complex from *S. macescens* 7AJQ. the red and orange densities are from ExbD TM helices. The black lines indicate the level of the micelle and the red lines show the level of the inner lipid densities in ExbB and of ExbD TM in the complex.

bacterial RND trimers

The bacterial RND family members are trimers and, similarly to eukaryotic RND members, the monomer has a 12 trans-membrane helical domain and two periplasmic domains with similar folds, resulting from a gene duplication. The archetype of the family is the antibiotic-resistance pump AcrB, whose crystal structure 2DHH showed the rotation between 3 ligand states present in the trimer and disclosed the transport mechanism [37]. The 2.8Å resolution 2Fo-Fc map from this structure shows no ordered lipid. On the other hand, the 3.17Å resolution SP-TEM structure of AcrB in proteo-lipid nanodiscs 6SGR [38] is rich in lipids even though the deposited model only contains protein residues (figure 9 A). The density map shows the micelle and a few ordered lipids at the interface between 2 AcrB monomers (figure 9 B). The core of the AcrB trimer hosts a lipid bilayer that pack in a pseudo-hexagonal arrangement (figure 9 C-D). This symmetrical arrangement exists even though no symmetry was imposed during map calculation. As observed for the external region of the TM region, the rim of the pore is surrounded by positively charged aminoacids on the cytoplasmic side and apolar inside. It is likely that lipids first interact with the protein and then form lipid-lipid contacts inside the pore. Structures from related proteins such as CusA trimer 7KF7 [39] or AdeJ 7RY3 [40] show similar

lipid arrangement. RND drug efflux in gram-negative bacteria operates via a two-membrane spanning machinery such as the OprM-MexA-MexB complex 6TA5, orthologous to AcrA-AcrB-TolC. In this structure, the MexB IM trimer is filled with lipid similarly to that of AcrB [41].

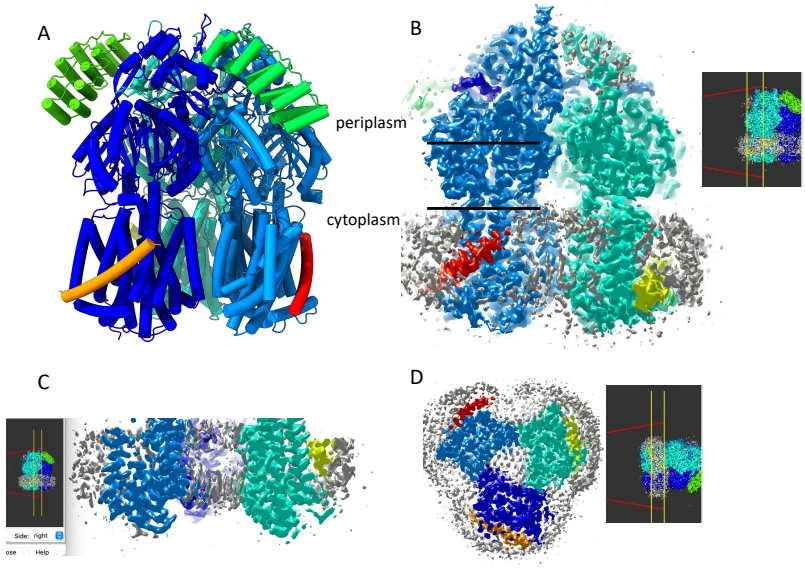

Figure 9
Bacterial RND transporter family. A-D, AcrB-Z structure 6SGR. A, molecular model of AcrB trimer (cyan, blue, dark blue) bound to one AcrZ helix in the TM region (red, yellow, orange). B, overall density traced at level 2 shows a micelle and a few ordered lipids at the interface between AcrB monomers. C, the core of the trimer shows an ordered bilayer with more order in the cytoplasmic leaflet. D. this bilayer has almost crystalline order as seen from the top. The figures on black background show the protein slice of the corresponding image.

Hexameric proteins with ordered lipidic region

The plasma membrane of *Saccharomyces cerevisiae* contains microdomains, including a sphingolipid-rich compartment containing proton ATPase Pma1. Single particle SP-TEM structure 7VH6 of Pma1 revealed a hexameric structure with 10 helical TM domains per monomer, an actuator domain, a nucleotide-binding domain and a phosphorylation domain. The trans-membrane hexamer forms a very peculiar “lake” that hosts 57 phospholipids in the extracellular leaflet with a pseudo-hexagonal packing (figures 10 A and B) [42]. The aliphatic chains are very tightly packed and as a consequence, their density is very clear. The central lipids have very straight density suggesting that they are totally saturated, while those in contact with the protein bend towards it and are likely unsaturated [42]. The inner leaflet has density visible at contour level 2, but it is disordered (figure 10 C). Pma1 is thought to organize membrane lipid microdomains via a currently unknown mechanism.

The acid-activated urea channel of *Helicobacter pylori* is a very specific feature of this bacterium causative of gastric diseases and cancers. When activated by acidic stomach conditions, the IM channel allows urea entry that is then degraded by urease into ammonia and carbonic acid, thus buffering the periplasmic space and allowing survival of the bacterium. The protein structure 6NSJ [43] (figures 10-D and E) is a hexamer in which each monomer forms a 6-helix channel surrounding a central hydrophobic tunnel that contains ordered lipids. Although the cytoplasmic leaflet of this tunnel is better ordered, the whole bilayer is well-defined (figure 10-F). The role of those lipids is not discussed in the above reference, but it is tempting to compare them structurally to the central region of hexameric Pma1.

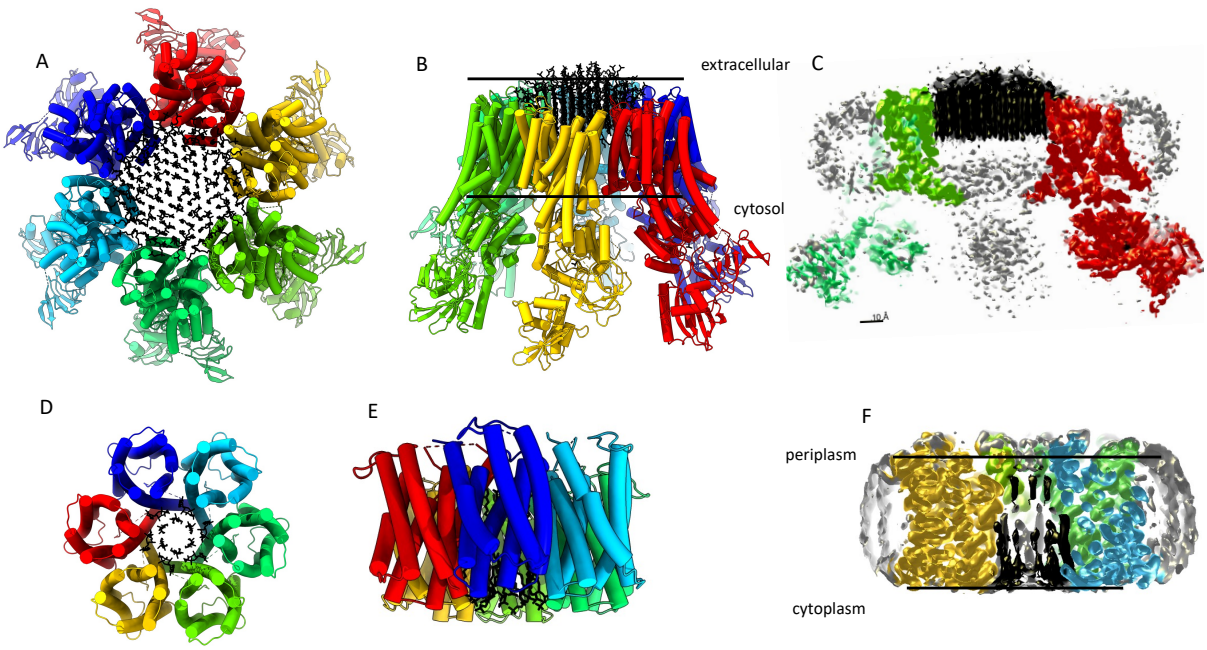

Figure 10
Proteins with ordered lipids in the core. A-C, plasma membrane ATPase1 PDB code 7VH6. A and B, model with chains colored as rainbow and lipids in black. C, density map traced at level 2 colored according to model shows an ordered lipid monolayer in the extracellular leaflet of the protein core. D-F, bacterial urea channel PDB code 6NSJ. D-E, model with chains colored as rainbow and lipids in black. F, density map traced at level 2 colored according to model shows an ordered lipid bilayer in the protein core.

Finally, as was mentioned above, MscS also contains lipid-like density inside its heptameric channel (figure 5 C and G).

In summary, many proteins form a hydrophobic tunnel large enough to contain several lipids that organize as a bilayer. Some of them are thought to be involved in lipid sorting and the organization of membrane sub-domains.

Mechanical role of protein-lipid interaction: membrane-bending proteins

- Solute carrier family SLC

- Prestin, a member of the solute carrier family 26 (SLC26) of anion transporters is the electromotive signal amplifier protein of outer hair cells. As a mechano-sensitive motor it senses both voltage and membrane tension and is involved in hearing and heart-beat regulation [44]. Prestin is a domain-swapped homodimer with a membrane domain and a cytoplasmic domain. Lipids are very important in Prestin's function as it triggers a membrane remodelling upon its activation. Most SP-TEM structures, as exemplified by Chloride-bound structure of Prestin in nanodisc (PDB ID: 7LGU) [45], show very clear density for a bilayer across the transmembrane region. The density is that of phospholipid in the annular region and of cholesterol in the interface between the 2 monomers in the membrane area (figure 11 A-B). In relationship with the membrane deformation role of the protein, the belt formed by annular lipids is not straight around the protein, but is deeper at the dimer interface. Salicylic acid triggers a change in the trans-membrane domain of Prestin in detergent glycol diosgenin (GDN) (structure 7LH2 from the same group) [45] (figure 11 C-D). The bilayer is straighter and the cholesterol is bound less deep in the cleft between the monomers as a result of the cleft closure. It is likely that

the radius of curvature of the surrounding membrane is different between both states. The Prestin structure is very similar to that of Solute Carrier 26 family member A9 (SLC26-9), an anion transporter PDB ID: 7CH1 [46]. Although no lipid was built in the chloride-bound model, a clear bilayer is visible in the SP-TEM map (figures 11 E-F) with a shape equivalent to that of Prestin 7LGU. Remarkably, map superposition shows that lipids visible in maps associated to 7GLU, 7LH2 and 7CH1 are bound at similar sites on the protein, showing that they are discrete binding sites (figure 11 G). Another member of SLC26 family is the Sulfate Transporter SULTR from *Arabidopsis thaliana*. Its SO_4^{2-} bound structure in GDN (PDB ID: 7LHV) [47] also shows a bilayer-like shape, although it is not as clear as the other structures (not illustrated).

- KCC potassium-coupled chloride transporter (SLC12 family)

Potassium-coupled chloride transporters (KCCs) mediate neutral transport in the same direction of chloride and potassium or sodium ions. They play crucial roles in regulating cell volume and intracellular chloride concentration, particularly in blood pressure regulation and kidney filtration. Those homodimers are characteristically inhibited under isotonic conditions via phospho-regulatory sites located within the cytoplasmic termini.

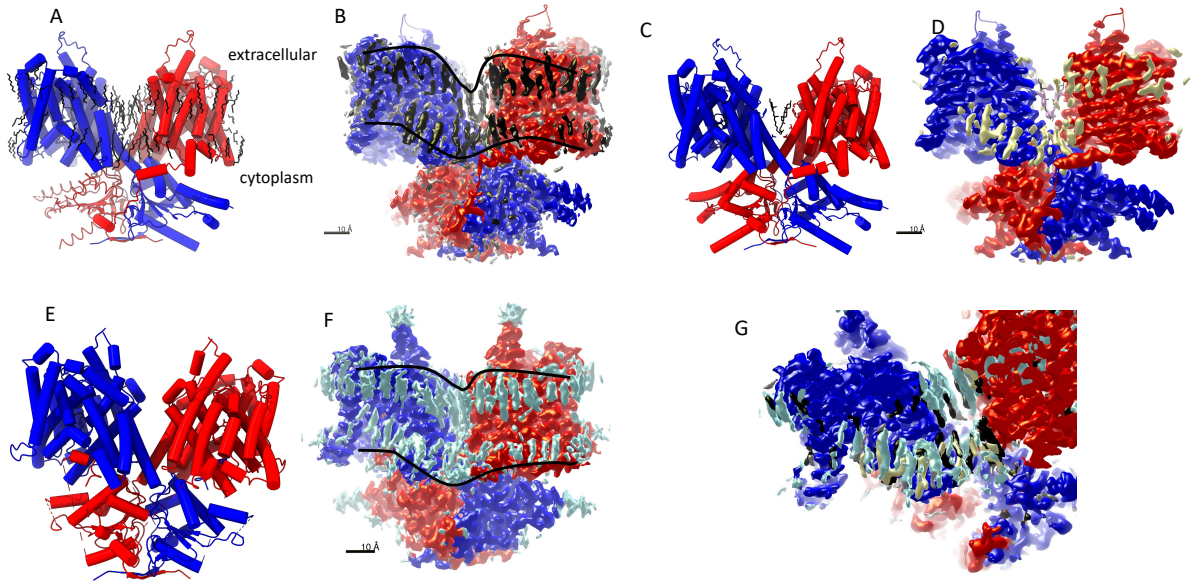

Figure 11
Prestin and SLC26 family distort membrane. A-B, prestin bound to Chloride ion 7LGU structure. A, molecular model with subunits colored blue and red and non-protein atoms in black. B, cryo-em map traced at level 1 colored according to model; grey regions are not modelled. The black lines follow the lipid bilayer shape. C-D, Structure 7LH2: Prestin bound to salicylic acid, same comments as for 7LGU. E-F, structure 7CH1, SLC26-9 carrier. No lipid was built in the map and the glacier-blue regions on figure F describe a lipid bilayer as traced by the black lines. G, superimposition of structures 7LGU, 7LH2 and 7CH1 shows that many lipids in the lower bilayer are in the same location with respect to the blue monomer.

As for Prestin, a structure of KCC3 (PDB ID: 6M22) [48] shows the homodimer in an inward-open conformation (figure 12 A) associated with ordered annular lipids forming a bent bilayer invaginated at the monomer interface with respect to the outer region (figure 12 B). A perpendicular view shows lipids in the dimer interface (figure 12 C). The black density is assigned to inhibitor [(dihydroindenyl) oxy] alkanoic acid. The structure of KCC1 (PDB ID: 6NPL [49]) is in a partially inward-open conformation where the two membrane domains are closer to each other with respect to 6M22 (figure 12 D). The

dimer interface shows ordered lipids that were traced in the model and the annular bilayer also has a bent shape, but is less invaginated than that of PDB ID: 6M22 (figure 12 E). The reason for this local membrane bending and its long-range consequences are not clear [50], and probably deserves further investigation.

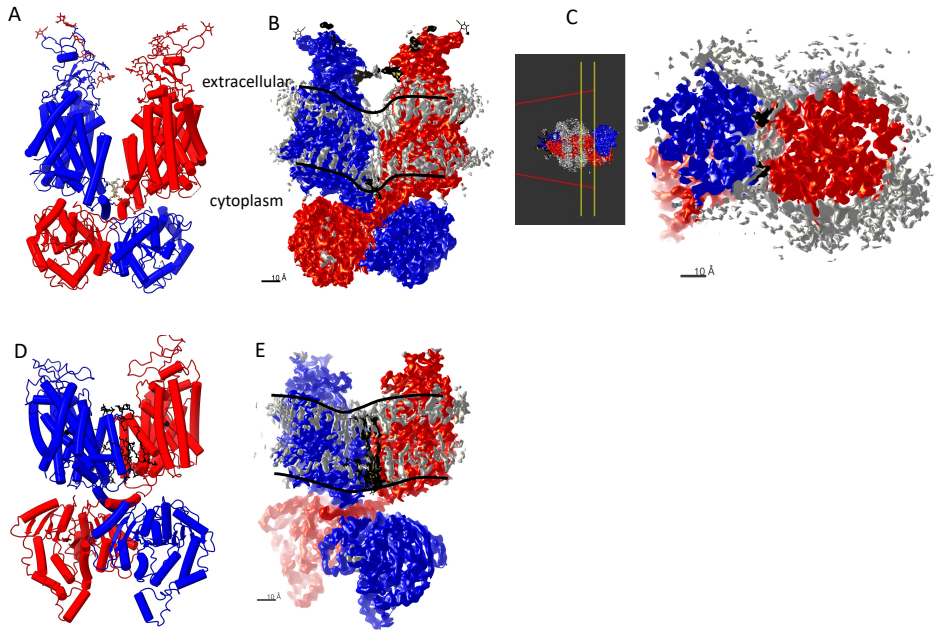

Figure 12
Annular lipids associated to solute carrier protein family KCC1 and KCC3 have a bent shape. A-C, KCC3 protein model 6M22 is in an open conformation. A, molecular model with subunits colored blue and red and non-protein atoms in black. B, cryo-em map (level 1) colored according to model; grey regions are not modelled. The black lines follow the lipid bilayer shape. C, slice across density map traced at level 2 in the membrane region shows ordered lipids between the two subunits. the inset shows the region where the slices were cut. D-E, KCC1 structure 6NPL, model and density map (level 1) with annular lipid trace.

In summary, the Solute carrier 26-9, SLC 12 and Prestin families interact very strongly with lipids and the shape of the bilayer in close contact with the protein seems to be important for membrane deformation and function of the protein. Cryo-electron tomography studies should reveal higher-order consequences of those protein-lipid interactions.

As mentioned above, Mitochondrial ATP synthase self-associates in a dimer that triggers membrane bending and curvature. Figure 4A shows the angle induced by the dimer assembly. In a larger scale, cryo-electron tomography studies showed that the dimers self-assemble on mitochondrial membranes or on proteoliposomes and induce membrane curvature to shape the crystae [51].

Conclusion

In the introduction, we compared the task of building lipid models in SP-TEM density to that of water molecules around hydrophilic proteins. However, water is by definition chemically homogeneous and simple to model, as a single oxygen atom is visible in X-ray crystallography maps. In some cases, the density can be assigned to an ion, that can be distinguished by its distances and its chelation geometry and/or its anomalous signal. Lipids are more similar to organic ligands with their charge, number of atoms and structural diversity. Still, the number of annular lipids is higher than ligands and

in this they can be compared to solvation water molecules. SP-TEM relies on averages of thousands of individual particles, that need to be similar enough to disclose atomic details of the protein that builds the reference structure and is the focus of the structural study. Lipids around the protein appear as a consequence of the protein order, but they may not have identical positions and conformations in all particles. As a result, the first 8-12 carbon atoms and sometimes the head group of the lipids in contact with the protein are often visible, while the rest of the aliphatic chain is disordered, thus making it difficult to distinguish between detergent such as dodecyl maltoside and lipids. Moreover, identification of the head group and estimation of the chain length and location of insaturations may be difficult due to fuzzy density. We saw in this review that SP-TEM is very good to locate and sometimes model tightly-bound lipids, and resolution improvement will probably enable a very precise model building including insaturation etc, provided that the protein selects a given lipid type at a given binding site.

The bilayer is often not visible or is more disordered in one leaflet than in the other one. We observed a difference in the quality of the lipid density according to the membrane leaflet and, although this is by no means statistically relevant, we found that the cytoplasmic leaflet in the maps we studied and illustrated was sometimes better ordered than the periplasmic or extracellular one. This may be related to the “positive inside” rule of TM helix dipole, that may stabilise negatively charged head groups. Headgroups are often more disordered than aliphatic chains. This may be due to their negative charge similar to acidic aminoacid side chains whose density is often truncated due to their interaction with electrons at medium density.

Annular lipids can be located precisely if the map resolution is better than 3Å, but SP-TEM maps will probably stay limited in their capacity to precisely model a complete annular shell, due to the disorder that we observe. In this respect, molecular dynamics is very useful to complement the model and obtain mechanistic information, for example for F0 ATPase motor [52] or the V0 proton channel [53]. In both cases, lipids were treated as surrounding (either explicitly or as bulk continuum) during the simulations to better understand the proton transfer mechanisms. The lipid pockets observed in the maps have not been modelled as yet and they deserve to be studied.

Most articles figures show high contour level density map representation (here defined as level 0 to 1), to exhibit protein details. This often omits lipids that are only visible at level 2. Just as high-resolution X-ray density maps show more water molecules, higher resolution SP-TEM maps reveal more lipid molecules, ligands, ions and water molecules and technical improvements will undoubtedly improve the visualisation. Methodological developments go more and more towards *in situ* observation of proteins using tomography and sub-tomogram averaging that allow higher and higher resolution to visualise sub-cellular regions such as the primary cilium, revealing details of the association between motor proteins and the membrane [54]; see [55] for a technical review. With resolution improvement, some lipids should become visible using sub-tomogram averaging in the near future. Also, more structures will probably be solved from proteins directly solubilised in SMA or amphipol, thus giving access to endogenous lipids or at least the lipids in which the protein is embedded during heterologous expression.

We found that some membrane protein families such as TRPV or SLC seem to bind lipids more strongly than others such as RND. It will be interesting to use complementary methods such as native mass spectroscopy to investigate if this is really the case, or if the lipids are less ordered and thus less visible in SP-TEM maps.

This review has limitations as it relies on the EMDB-deposited maps, and we decided to limit ourselves to those that can be downloaded via the PDB interface. Most of the time, the map is modified by sharpening mask to improve resolution in the membrane area. Now it is compulsory to deposit unmasked half maps, which could reveal more details and outline the mask effect, in particular when it is too tight and erases lipids.

This review highlights that SP-TEM maps of membrane proteins and complexes are rich in information about lipids that are sometimes overlooked by atomic models, but constitute precious information about protein-lipid interactions and could give access to part of the “paralipidome” of membrane proteins [56].

Acknowledgements

I thank the PDB and EMBD for making public protein structures and their associated density maps. I am old enough to remember that it used to be called the Brookhaven Protein Data Bank before it moved to Rutgers in 1998, and that European and Japanese sisters were made available. Those databases have been unique open-data repositories for a very long time and we structural biologists are proud to remember that we have made our work open long before it became a rule for other sciences. I thank Andrew Thompson (SOLEIL synchrotron, France) and Philippe Delepelaire (Institut de Biologie Physico-Chimique, CNRS, Paris) for critical reading of the manuscript and useful suggestions.

Funding

This work was supported by LABEX Dynamo (ANR-11-LABX-0011), and by Centre National de la Recherche Scientifique CNRS, France

Table 1

PDB entry	EMDB entry	Protein and organism	Resolution (Å)	Symmetry	reference
6DMY	7968	Protein Patched homolog 1 + Sonic Hedgehog *Homo sapiens*	3.6	C1	[57]
6M22	30058	Solute carrier family 12 member 6 KCC3 *Homo sapiens*	2.7	C2	[48]
6NPL	0473	NKCC1 Solute carrier family 12 member 2 *Danio rerio*	2.9	C2	[49]
6NSJ	0498	Acid-activated urea channel *Helicobacter pylori J99*	2.7	C6	[43]
6O1N	0593	Transient receptor potential cation channel subfamily V member 5 (TRPV5) *O. cuniculus*	2.9	C4	[18]
6RD4	4805	mitochondrial F-ATP synthase *Polytomella sp Pringsheim*	2.9	C2	[23]
6RLD	4919	mechanosensitive channel Mscs in membrane bilayer *E. coli*	2.93	C7	[58]
6S8G	10121	Lipopolysaccharide ABC transporter, subunits LptB, LptF, YigQ *Shigella flexneri*	3.5	C1	[27]
6S8H	10122	Lipopolysaccharide ABC transporter, subunits LptB, LptF, YigQ *Shigella flexneri*	3.7	C1	[27]
6S8N	10125	Lipopolysaccharide ABC transporter, subunits LptB, LptC and LptF; *Shigella flexneri*	3.1	C1	[27]
6SGR	10182	Multidrug efflux pump AcrB-AcrZ+ darpin *E. coli*	3.17	C1	[38]
6SM3	10241	TonB-dependent transporter RagA Lipoprotein RagB*Porphyromonas gingivalis*	3.2	C2	[59]
6TA5	10372	OprM-MexA-MexB RND transporter *Pseudomonas aeroginosa*	3.2	C3	[41]
6VYK	21462	Mechanosensitive channel MscS in PC-18:1 nanodiscs (closed) *E. coli*	3.2	C7	[25]
6VYL	21463	Mechanosensitive channel MscS in PC-10 nanodisc (partially open) *E. coli*	3.4	C7	[25]
6W6S	21546	Niemann-Pick type C NPC1 structure in GDN micelles at pH 8.0 *Homo sapiens*	3	C1	[33]
6YE4	10789	ExbB *Serratia marcescens*	3.2	C5	[6]
7AJQ	11806	ExbB-ExbD *S. marcescens*	4	C1	[6]
7CH1	30368	Solute carrier family 26 member 9 *Homo sapiens*	2.6	C2	[46]
7JG5	22311	ATP synthase *Mycobacterium smegmatis*	3.4	C1	[20]
7LGU	23329	Prestin *Homo sapiens*	2.3	C2	[45]
7LH2	23334	Prestin *Homo sapiens*	3.43	C2	[45]
7N4U	24178	NPC1L1 *Homo sapiens*	3.34	C2	[34]
7NK9	12434	ATP synthase Fo domain *M. smegmatis*	2.9	C1	[22]
7NL9	12461	ATP synthase Fo domain *M. smegmatis*	2.86	C1	[22]
7RHR	24467	Patched-1 *Xenopus calcaratus*	3	C1	[30]
7RPI	24615	Dispatched *Mus musculus*	2.5	C1	[31]
7S88	24890	Transient receptor potential cation channel subfamily V member 6 (TRPV6) *Homo sapiens*	2.69	C4	[17]
7VH6	31988	Plasma membrane H+ ATPase 1 *S. cerevisae*	3.8	C1	[42]

Table 1: list of structures and density maps used in this review.

Supplementary Table 1

PDB entry	Protein and organism	Resolution (Å)	ligands	reference
6DMY	Protein Patched homolog 1 + Sonic Hedgehog *Homo sapiens*	3.6	Y01, NAG	[57]
6M22	Solute carrier family 12 member 6 KCC3 *Homo sapiens*	2.7	NAG, EZC	[49]
6NPL	NKCC1 Solute carrier family 12 member 2 *Danio rerio*	2.9	POV	[50]
6NSJ	Acid-activated urea channel *Helicobacter pylori J99*	2.7	XP4	[44]
6O1N	Transient receptor potential cation channel subfamily V member 5 (TRPV5) *O. cuniculus*	2.9	None	[18]
6RD4	mitochondrial F-ATP synthase *Polytomella sp Pringsheim*	2.9	Zn, Mg, ATP, ADP	[23]
6RLD	mechanosensitive channel Mscs in membrane bilayer *E. coli*	2.93	PCW	[58]
6S8G	Lipopolysaccharide ABC transporter, subunits LptB, LptF, YigQ *Shigella flexneri*	3.5	ANP, LMD	[28]
6S8H	Lipopolysaccharide ABC transporter, subunits LptB, LptF, YigQ *Shigella flexneri*	3.7	JSG, LMN, LMT	[28]
6S8N	Lipopolysaccharide ABC transporter, subunits LptB, LptC and LptF; *Shigella flexneri*	3.1	DCQ, LMN, LMT, L0W	[28]
6SGR	Multidrug efflux pump AcrB-AcrZ+ darpin *E. coli*	3.17	None	[39]
6SM3	TonB-dependent transporter RagA Lipoprotein RagB*Porphyromonas gingivalis*	3.2	5PL, PLM	[59]
6TA5	OprM-MexA-MexB RND transporter *Pseudomonas aeroginosa*	3.2	None	[42]
6VYK	Mechanosensitive channel MscS in PC-18:1 nanodiscs (closed) *E. coli*	3.2	PCW	[26]
6VYL	Mechanosensitive channel MscS in PC-10 nanodisc (partially open) *E. coli*	3.4	None	[26]
6YE4	ExbB *Serratia marcescens*	3.2	PGT	[6]
7AJQ	ExbB-ExbD *S. marcescens*	4	None	[6]
7CH1	Solute carrier family 26 member 9 *Homo sapiens*	2.6	Na, Cl	[47]
7JG5	ATP synthase *Mycobacterium smegmatis*	3.4	ATP, ADP, Mg, PO4	[20]
7LGU	Prestin *Homo sapiens*	2.3	CL, CLR, OCT, D10, D12, HEX, HP6, C14	[46]
7LH2	Prestin *Homo sapiens*	3.43	CLR, SAL	[46]
7N4U	NPC1L1 *Homo sapiens*	3.34	CLR, NAG, VIV, POV	[35]
7NK9	ATP synthase Fo domain *M. smegmatis*	2.9	None	[22]
7NL9	ATP synthase Fo domain *M. smegmatis*	2.86	None	[22]
7RHR	Patched-1 *Xenopus calcaratus*	3	NAG, CLR	[31]
7RPI	Dispatched *Mus musculus*	2.5	AV0, NAG	[32]
7S88	Transient receptor potential cation channel subfamily V member 6 (TRPV6) *Homo sapiens*	2.69	PCW, POV	[17]
7VH6	Plasma membrane H+ ATPase 1 *S. cerevisae*	3.8	POV	[43]

Suppl Table 1 list of ligands modeled in PDB files.

AV0 2,2-DIDECYLPROPANE-1,3-BIS-B-D-MALTOPYRANOSIDE
C14 TETRADECANE
CL CHLORIDE ION
CLR CHOLESTEROL
D10 DECANE
D12 DODECANE
EZC 2-[[(2~{R})-2-BUTYL-6,7-BIS(CHLORANYL)-2-CYCLOPENTYL-1-2 EZC OXIDANYLIDENE-3~{H}-INDEN-5-YL]OXY]ETHANOIC ACID= DIOA
HEX HEXANE
HP6 HEPTANE
JSG lipopolysaccharide fragment

L0W LIPOPOLYSACCHARIDE FRAGMENT
LMD TETRADECYL 4-O-ALPHA-D-GLUCOPYRANOSYL-BETA-D- GLUCOPYRANOSIDE
LMN LAURYL MALTOSE NEOPENTYL GLYCOL
LMT DODECYL-BETA-D-MALTOSIDE
NAG 2-ACETAMIDO-2-DEOXY-BETA-D-GLUCOPYRANOSE
OCT N-OCTANE
PCW 1,2-DIOLEOYL-SN-GLYCERO-3-PHOSPHOCHOLINE
PGT phosphatidyl-glycerol
PLM PALMITIC ACID
POV (2S)-3-(HEXADECANOYLOXY)-2-[(9Z)-OCTADEC-9- 2 ENOYLOXY]PROPYL 2(TRIMETHYLAMMONIO)ETHYL PHOSPHATE = POPC
5PL (1R,4S,6R)-6-({[2-(ACETYLAMINO)-2-DEOXY-ALPHA-D-GLUCOPYRANOSYL]OXY}METHYL)-4-HYDROXY-1-{[(15-METHYLHEXADECANOYL)OXY]METHYL}-4-OXIDO-7-OXO-3,5- DIOXA-8-AZA-4-PHOSPHAHEPTACOS-1-YL 15-METHYLHEXADECANOATE
SAL 2-HYDROXYBENZOIC ACID= SALICYLIC ACID
VIV (2R)-2,5,7,8-TETRAMETHYL-2-[(4R,8R)-4,8,12- TRIMETHYLTRIDECYL]CHROMAN-6-OL (2S)-3-(HEXADECANOYLOXY)-2-[(9Z)-OCTADEC-9-
XP4 1,2-DIMYRISTOYL-SN-GLYCERO-3-PHOSPHATE
Y01 CHOLESTEROL HEMISUCCINATE

References

[1] J.R. Brotherus, O.H. Griffith, M.O. Brotherus, P.C. Jost, J.R. Silvius, L.E. Hokin, Lipid-protein multiple binding equilibriums in membranes, Biochemistry, 20 (1981) 5261–5267.

[2] D. Marsh, L.I. Horváth, Structure, dynamics and composition of the lipid-protein interface Perspectives from spin-labelling, Biochim. Biophys. Acta BBA - Rev. Biomembr., 1376 (1998) 267–296.

[3] H. Palsdottir, C. Hunte, Lipids in membrane protein structures, Biochim. Biophys. Acta BBA - Biomembr., 1666 (2004) 2–18.

[4] K. Xue, K.T. Movellan, X.C. Zhang, E.E. Najbauer, M.C. Forster, S. Becker, L.B. Andreas, Towards a native environment: structure and function of membrane proteins in lipid bilayers by NMR, Chem. Sci., 12 (2021) 14332–14342.

[5] J.R. Bolla, M.T. Agasid, S. Mehmood, C.V. Robinson, Membrane Protein-Lipid Interactions Probed Using Mass Spectrometry, Annu. Rev. Biochem., 88 (2019) 85–111.

[6] V. Biou, R.J.D. Adaixo, M. Chami, P.-D. Coureux, B. Laurent, V.Y.N. Enguéné, G.C. de Amorim, N. Izadi-Pruneyre, C. Malosse, J. Chamot-Rooke, H. Stahlberg, P. Delepelaire, Structural and molecular determinants for the interaction of ExbB from Serratia marcescens and HasB, a TonB paralog, Commun. Biol., 5 (2022) 1–15.

[7] A. Camara-Artigas, D. Brune, J.P. Allen, Interactions between lipids and bacterial reaction centers determined by protein crystallography, Proc. Natl. Acad. Sci., 99 (2002) 11055–11060.

[8] P. Kumar, G.D. Cymes, C. Grosman, Structure and function at the lipid–protein interface of a pentameric ligand-gated ion channel, Proc. Natl. Acad. Sci., 118 (2021).

[9] A. Marconnet, B. Michon, C. Le Bon, F. Giusti, C. Tribet, M. Zoonens, Solubilization and Stabilization of Membrane Proteins by Cycloalkane-Modified Amphiphilic Polymers, Biomacromolecules, 21 (2020) 3459–3467.

[10] M. Tagari, R. Newman, M. Chagoyen, J.M. Carazo, K. Henrick, New electron microscopy database and deposition system, Trends Biochem. Sci., 27 (2002) 589.

[11] H.M. Berman, J. Westbrook, Z. Feng, G. Gilliland, T.N. Bhat, H. Weissig, I.N. Shindyalov, P.E. Bourne, The Protein Data Bank, Nucleic Acids Res., 28 (2000) 235–242.

[12] T.D. Goddard, C.C. Huang, E.C. Meng, E.F. Pettersen, G.S. Couch, J.H. Morris, T.E. Ferrin, UCSF ChimeraX: Meeting modern challenges in visualization and analysis, Protein Sci. Publ. Protein Soc., 27 (2018) 14–25.

[13] E.F. Pettersen, T.D. Goddard, C.C. Huang, G.S. Couch, D.M. Greenblatt, E.C. Meng, T.E. Ferrin, UCSF Chimera--a visualization system for exploratory research and analysis, J Comput Chem, 25 (2004) 1605–12.

[14] V. Zampieri, A. Gobet, X. Robert, P. Falson, V. Chaptal, CryoEM reconstructions of membrane proteins solved in several amphipathic solvents, nanodisc, amphipol and detergents, yield amphipathic belts of similar sizes corresponding to a common ordered solvent layer, Biochim. Biophys. Acta BBA - Biomembr., 1863 (2021) 183693.

[15] Z. Deng, N. Paknejad, G. Maksaev, M. Sala-Rabanal, C.G. Nichols, R.K. Hite, P. Yuan, Cryo-EM and X-ray structures of TRPV4 reveal insight into ion permeation and gating mechanisms, Nat. Struct. Mol. Biol., 25 (2018) 252–260.

[16] M.K. van Goor, L. de Jager, Y. Cheng, J. van der Wijst, High-resolution structures of transient receptor potential vanilloid channels: Unveiling a functionally diverse group of ion channels, Protein Sci., 29 (2020) 1569–1580.
[17] A. Neuberger, K.D. Nadezhdin, A.I. Sobolevsky, Structural mechanisms of TRPV6 inhibition by ruthenium red and econazole, Nat. Commun., 12 (2021) 6284.
[18] S. Dang, M.K. van Goor, D. Asarnow, Y. Wang, D. Julius, Y. Cheng, J. van der Wijst, Structural insight into TRPV5 channel function and modulation, Proc. Natl. Acad. Sci., 116 (2019) 8869–8878.
[19] J.E. Walker, ATP Synthesis by Rotary Catalysis (Nobel lecture), Angew. Chem. Int. Ed., 37 (1998) 2308–2319.
[20] H. Guo, G.M. Courbon, S.A. Bueler, J. Mai, J. Liu, J.L. Rubinstein, Structure of mycobacterial ATP synthase bound to the tuberculosis drug bedaquiline, Nature, 589 (2021) 143–147.
[21] W. Kühlbrandt, Structure and Mechanisms of F-Type ATP Synthases, Annu. Rev. Biochem., 88 (2019) 515–549.
[22] M.G. Montgomery, J. Petri, T.E. Spikes, J.E. Walker, Structure of the ATP synthase from Mycobacterium smegmatis provides targets for treating tuberculosis, Proc. Natl. Acad. Sci., 118 (2021) e2111899118.
[23] B.J. Murphy, N. Klusch, J. Langer, D.J. Mills, Ö. Yildiz, W. Kühlbrandt, Rotary substates of mitochondrial ATP synthase reveal the basis of flexible F1-Fo coupling, Science, 364 (2019) eaaw9128.
[24] C. Pliotas, A.C.E. Dahl, T. Rasmussen, K.R. Mahendran, T.K. Smith, P. Marius, J. Gault, T. Banda, A. Rasmussen, S. Miller, C.V. Robinson, H. Bayley, M.S.P. Sansom, I.R. Booth, J.H. Naismith, The role of lipids in mechanosensation, Nat. Struct. Mol. Biol., 22 (2015) 991–998.
[25] Y. Zhang, C. Daday, R.-X. Gu, C.D. Cox, B. Martinac, B.L. de Groot, T. Walz, Visualization of the mechanosensitive ion channel MscS under membrane tension, Nature, 590 (2021) 509–514.
[26] T.W. Owens, R.J. Taylor, K.S. Pahil, B.R. Bertani, N. Ruiz, A.C. Kruse, D. Kahne, Structural basis of unidirectional export of lipopolysaccharide to the cell surface, Nature, 567 (2019) 550–553.
[27] X. Tang, S. Chang, Q. Luo, Z. Zhang, W. Qiao, C. Xu, C. Zhang, Y. Niu, W. Yang, T. Wang, Z. Zhang, X. Zhu, X. Wei, C. Dong, X. Zhang, H. Dong, Cryo-EM structures of lipopolysaccharide transporter LptB2FGC in lipopolysaccharide or AMP-PNP-bound states reveal its transport mechanism, Nat. Commun., 10 (2019) 4175.
[28] M. Bidet, O. Joubert, B. Lacombe, M. Ciantar, R. Nehmé, P. Mollat, L. Brétillon, H. Faure, R. Bittman, M. Ruat, I. Mus-Veteau, The Hedgehog Receptor Patched Is Involved in Cholesterol Transport, PLoS ONE, 6 (2011) e23834.
[29] L. Signetti, N. Elizarov, M. Simsir, A. Paquet, D. Douguet, F. Labbal, D. Debayle, A. Di Giorgio, V. Biou, C. Girard, M. Duca, L. Bretillon, C. Bertolotto, B. Verrier, S. Azoulay, I. Mus-Veteau, Inhibition of Patched Drug Efflux Increases Vemurafenib Effectiveness against Resistant BrafV600E Melanoma, Cancers, 12 (2020).
[30] P. Huang, B.M. Wierbowski, T. Lian, C. Chan, S. García-Linares, J. Jiang, A. Salic, Structural basis for catalyzed assembly of the Sonic hedgehog–Patched1 signaling complex, Dev. Cell, 57 (2022) 670-685.e8.
[31] Q. Wang, D.E. Asarnow, K. Ding, R.K. Mann, J. Hatakeyama, Y. Zhang, Y. Ma, Y. Cheng, P.A. Beachy, Dispatched uses Na+ flux to power release of lipid-modified Hedgehog, Nature, (2021) 1–5.

[32] S.R. Pfeffer, NPC intracellular cholesterol transporter 1 (NPC1)-mediated cholesterol export from lysosomes, J. Biol. Chem., 294 (2019) 1706–1709.
[33] H. Qian, X. Wu, X. Du, X. Yao, X. Zhao, J. Lee, H. Yang, N. Yan, Structural Basis of Low-pH-Dependent Lysosomal Cholesterol Egress by NPC1 and NPC2, Cell, 182 (2020) 98-111.e18.
[34] T. Long, Y. Liu, Y. Qin, R.A. DeBose-Boyd, X. Li, Structures of dimeric human NPC1L1 provide insight into mechanisms for cholesterol absorption, Sci. Adv., 7 (2021) eabh3997.
[35] M. Santiveri, A. Roa-Eguiara, C. Kühne, N. Wadhwa, H. Hu, H.C. Berg, M. Erhardt, N.M.I. Taylor, Structure and Function of Stator Units of the Bacterial Flagellar Motor, Cell, 183 (2020) 244-257.e16.
[36] H. Celia, I. Botos, X. Ni, T. Fox, N. De Val, R. Lloubes, J. Jiang, S.K. Buchanan, Cryo-EM structure of the bacterial Ton motor subcomplex ExbB–ExbD provides information on structure and stoichiometry, Commun. Biol., 2 (2019).
[37] S. Murakami, R. Nakashima, E. Yamashita, T. Matsumoto, A. Yamaguchi, Crystal structures of a multidrug transporter reveal a functionally rotating mechanism, Nature, 443 (2006) 173–179.
[38] D. Du, A. Neuberger, M.W. Orr, C.E. Newman, P.-C. Hsu, F. Samsudin, A. Szewczak-Harris, L.M. Ramos, M. Debela, S. Khalid, G. Storz, B.F. Luisi, Interactions of a Bacterial RND Transporter with a Transmembrane Small Protein in a Lipid Environment, Structure, 28 (2020) 625-634.e6.
[39] M.A. Moseng, M. Lyu, T. Pipatpolkai, P. Glaza, C.C. Emerson, P.L. Stewart, P.J. Stansfeld, E.W. Yu, Cryo-EM Structures of CusA Reveal a Mechanism of Metal-Ion Export, MBio, 12 (2021) e00452-21.
[40] C.E. Morgan, Z. Zhang, R.A. Bonomo, E.W. Yu, An Analysis of the Novel Fluorocycline TP-6076 Bound to Both the Ribosome and Multidrug Efflux Pump AdeJ from Acinetobacter baumannii, MBio, (2022) e0373221.
[41] M. Glavier, D. Puvanendran, D. Salvador, M. Decossas, G. Phan, C. Garnier, E. Frezza, Q. Cece, G. Schoehn, M. Picard, J.-C. Taveau, L. Daury, I. Broutin, O. Lambert, Antibiotic export by MexB multidrug efflux transporter is allosterically controlled by a MexA-OprM chaperone-like complex, Nat. Commun., 11 (2020) 4948.
[42] P. Zhao, C. Zhao, D. Chen, C. Yun, H. Li, L. Bai, Structure and activation mechanism of the hexameric plasma membrane H+-ATPase, Nat. Commun., 12 (2021) 6439.
[43] Y. Cui, K. Zhou, D. Strugatsky, Y. Wen, G. Sachs, Z.H. Zhou, K. Munson, pH-dependent gating mechanism of the Helicobacter pylori urea channel revealed by cryo-EM, Sci. Adv., 5 (2022) eaav8423.
[44] X.-D. Zhang, P.N. Thai, L. Ren, M.C. Perez Flores, H.A. Ledford, S. Park, J.H. Lee, C.-R. Sihn, C.-W. Chang, W.C. Chen, V. Timofeyev, J. Zuo, J.W. Chan, E.N. Yamoah, N. Chiamvimonvat, Prestin amplifies cardiac motor functions, Cell Rep., 35 (2021) 109097.
[45] J. Ge, J. Elferich, S. Dehghani-Ghahnaviyeh, Z. Zhao, M. Meadows, H. von Gersdorff, E. Tajkhorshid, E. Gouaux, Molecular mechanism of prestin electromotive signal amplification, Cell, 184 (2021) 4669-4679.e13.
[46] X. Chi, X. Jin, Y. Chen, X. Lu, X. Tu, X. Li, Y. Zhang, J. Lei, J. Huang, Z. Huang, Q. Zhou, X. Pan, Structural insights into the gating mechanism of human SLC26A9 mediated by its C-terminal sequence, Cell Discov., 6 (2020) 1–10.
[47] L. Wang, K. Chen, M. Zhou, Structure and function of an Arabidopsis thaliana sulfate transporter, Nat. Commun., 12 (2021) 4455.
[48] X. Chi, X. Li, Y. Chen, Y. Zhang, Q. Su, Q. Zhou, Cryo-EM structures of the full-length human KCC2

and KCC3 cation-chloride cotransporters, Cell Res., 31 (2021) 482–484.
[49] T.A. Chew, B.J. Orlando, J. Zhang, N.R. Latorraca, A. Wang, S.A. Hollingsworth, D.-H. Chen, R.O. Dror, M. Liao, L. Feng, Structure and mechanism of the cation–chloride cotransporter NKCC1, Nature, 572 (2019) 488–492.
[50] T.A. Chew, J. Zhang, L. Feng, High-Resolution Views and Transport Mechanisms of the NKCC1 and KCC Transporters, J. Mol. Biol., 433 (2021) 167056.
[51] T.B. Blum, A. Hahn, T. Meier, K.M. Davies, W. Kühlbrandt, Dimers of mitochondrial ATP synthase induce membrane curvature and self-assemble into rows, Proc. Natl. Acad. Sci., 116 (2019) 4250–4255.
[52] S. Kubo, T. Niina, S. Takada, Molecular dynamics simulation of proton-transfer coupled rotations in ATP synthase FO motor, Sci. Rep., 10 (2020) 8225.
[53] S.-H. Roh, M. Shekhar, G. Pintilie, C. Chipot, S. Wilkens, A. Singharoy, W. Chiu, Cryo-EM and MD infer water-mediated proton transport and autoinhibition mechanisms of Vo complex, Sci. Adv., (2020).
[54] P. Kiesel, G. Alvarez Viar, N. Tsoy, R. Maraspini, P. Gorilak, V. Varga, A. Honigmann, G. Pigino, The molecular structure of mammalian primary cilia revealed by cryo-electron tomography, Nat. Struct. Mol. Biol., 27 (2020) 1115–1124.
[55] M. Turk, W. Baumeister, The promise and the challenges of cryo-electron tomography, FEBS Lett., 594 (2020) 3243–3261.
[56] I. Levental, E. Lyman, Regulation of membrane protein structure and function by their lipid nano-environment, Nat. Rev. Mol. Cell Biol., (2022) 1–16.
[57] X. Gong, H. Qian, P. Cao, X. Zhao, Q. Zhou, J. Lei, N. Yan, Structural basis for the recognition of Sonic Hedgehog by human Patched1, Science, (2018) eaas8935.
[58] T. Rasmussen, V.J. Flegler, A. Rasmussen, B. Böttcher, Structure of the Mechanosensitive Channel MscS Embedded in the Membrane Bilayer, J. Mol. Biol., 431 (2019) 3081–3090.
[59] M. Madej, J.B.R. White, Z. Nowakowska, S. Rawson, C. Scavenius, J.J. Enghild, G.P. Bereta, K. Pothula, U. Kleinekathoefer, A. Baslé, N.A. Ranson, J. Potempa, B. van den Berg, Structural and functional insights into oligopeptide acquisition by the RagAB transporter from Porphyromonas gingivalis, Nat. Microbiol., 5 (2020) 1016–1025.